

Evolution of the Black Hole Mass Function in Star Clusters from Multiple Mergers

PIERRE CHRISTIAN,¹ PHILIP MOCZ,² AND ABRAHAM LOEB¹

¹*Astronomy Department, Harvard University, 60 Garden St., Cambridge, MA 02138*

²*Department of Astrophysical Sciences, Princeton University, 4 Ivy Lane, Princeton, NJ, 08544, USA**

ABSTRACT

We investigate the effects of black hole mergers in star clusters on the black hole mass function. As black holes are not produced in pair-instability supernovae, it is suggested that there is a dearth of high mass stellar black holes. This dearth generates a gap in the upper end of the black hole mass function. Meanwhile, parameter fitting of X-ray binaries suggests the existence of a gap in the mass function under 5 solar masses. We show, through evolving a coagulation equation, that black hole mergers can appreciably fill the upper mass gap, and that the lower mass gap generates potentially observable features at larger mass scales. We also explore the importance of ejections in such systems and whether dynamical clusters can be formation sites of intermediate mass black hole seeds.

1. INTRODUCTION

The discovery of merging black holes (BHs) by the Laser Interferometer Gravitation-Wave Observatory (LIGO) signaled the beginning of gravitational wave astrophysics (Abbott et al. 2016b,a, 2017a,c,b). The masses of these binaries are much larger than those previously discovered as X-ray binaries (Özel et al. 2010; Farr et al. 2011; Kreidberg et al. 2012). The existence of these massive BHs was anticipated by previous calculations of BH mergers (Belczynski et al. 2010a,b; Dominik et al. 2015), and their detection spurred a growing interest on their formation mechanisms. One promising mechanism that allows binary BHs of such masses to form is the dynamical merger scenario, where BHs in dense star clusters gravitationally interact with each other to produce very hard binaries (O’Leary et al. 2006; Rodriguez et al. 2015, 2016a,b; Sukhbold et al. 2016; Samsing et al. 2018).

In such systems, BHs borne out of mergers can merge again producing second generation BHs (Antonini & Rasio 2016; Gerosa & Berti 2017; Fishbach et al. 2017; Rodriguez et al. 2017). These multiple mergers necessarily increase the number of massive BHs while simultaneously lowering the number of less massive BHs, turning the BH mass function (BHMF) more top-heavy in the process.

Supernova theory also predicts the existence of a mass gap in the BH initial mass function (IMF) between 50–130 M_{\odot} because the stellar progenitors of BHs in this mass range undergo pair-instability supernovae (Belczynski et al. 2016; Woosley 2017). Recently, parameter fitting of four LIGO data points suggests the existence of a cutoff at $M \sim 40M_{\odot}$, bolstering the validity of this theoretical calculation (Fishbach & Holz 2017). Further, more massive binary BHs can be observed by LIGO to a greater distance, and so the absence of LIGO events at $M \gtrsim 40M_{\odot}$ within the increased survey volume can be used to set an upper limit on the BHMF. Analysis on the redshift distribution of LIGO events corroborates the existence of this mass gap (Bai et al. 2018).

In the dynamical merger scenario, multiple merger events might be able to appreciably fill the upper mass gap. In addition, while binary BHs in isolated binaries can merge to produce BHs in the upper mass gap, the lack of multiple merger events results in a very different BHMF within the upper mass gap. As such, the BHMF within the upper mass gap could be an effective test for the dynamical merger scenario.

Finally, parameter fitting of X-ray binaries suggests the existence of a lower mass gap in the BHMF between the most massive neutron stars and the least massive BHs (Özel et al. 2010; Farr et al. 2011). Under certain scenarios, supernova explosions can naturally produce this gap (Belczynski et al. 2012). According to Ref. Belczynski et al. (2012), Rayleigh-Taylor instabilities could appear early after the initial bounce of a supernova, and drive explosions $\lesssim 100 - 200$ ms after the collapse. In such rapid explosions, stars of mass $\sim 14 - 20M_{\odot}$ are

Corresponding author: Pierre Christian
pchristian@cfa.harvard.edu

* Einstein Fellow

thought to produce strong explosions that result in high mass neutron stars ($M \sim 1.5 - 2M_\odot$). However, stars of mass $\sim 20 - 40M_\odot$ fail to explode in this scenario, forming BHs of mass $M \sim 5 - 10M_\odot$.

This gap has also been successfully reproduced by numerical simulations of neutrino-driven supernova explosions (Sukhbold et al. 2016). Neutrino-driven explosions suggests that smaller stars never implode to form BHs, a prediction that has also been corroborated by the observed BH and neutron star distributions (Raithel et al. 2017). If multiple mergers are allowed, the lack of BHs in this range will have repercussions to the BHMF even at larger mass scales, as heavier BHs cannot merge with BHs in the lower mass gap to produce more massive BHs.

To answer such questions, a method to quickly compute the evolution of the BHMF is needed. In this work, we will employ the Smoluchowski coagulation equation Smoluchowsky (1916), a rate equation describing the time evolution of the number of particles of a certain size as the particles are allowed to interact and ‘coagulate’, merging to form larger particles. The calculations performed in this formalism are much faster than those required in N-body simulations of dynamical clusters, allowing a large parameter space to be covered efficiently.

This paper is organized as follows: in Section 2 we describe the Smoluchowski coagulation equation formalism, in Section 3 we discuss our results for the evolution of the BHMF assuming constant kernel. Subsequently Section 4 presents our results with top-heavy kernels. Finally Section 5 summarizes our conclusions.

2. METHODS

The evolution of the BH mass function due to mergers can be modeled by a coagulation equation,

$$\begin{aligned} \frac{\partial N(M, t)}{\partial t} = & \\ & \frac{1}{2} \int_0^M K(M - M', M') N(M - M', t) N(M', t) dM' \\ & - \int_0^\infty K(M, M') N(M, t) N(M', t) dM' - S(M, t), \end{aligned} \quad (1)$$

where $N(M, t)dM$ is the number of black holes in the star cluster of mass $\in [M, M + dM]$ at time t , $K(x, y)$ – the *coagulation kernel* – is the rate of two BHs of masses x and y to merge, and $S(M, t)$ represents possible source or sink terms. The first term of this equation describes BHs of mass $< M$ merging to form BHs of mass M , while the second term describes removal of BHs of mass M merging to form BHs with mass $> M$.

Equation (1) is called the Smoluchowsky (1916) coagulation equation, a general integro-differential equation that describes the statistical time-evolution of the distribution (as a function of mass, size, etc.) of a coagulating population of objects. The detailed physics of the coagulation process is encoded in the coagulation kernel, allowing one to just evolve the statistical ensemble. The numerical method used to solve Equation (1) is described in Appendix A.

We solve the coagulation equation for a variety of physical scenarios, and study its evolution over 10 Gyrs. Our IMF follows the Salpeter function ($N \propto M^\alpha$, $\alpha = -2.35$; Salpeter 1955) with an upper mass gap for $50M_\odot < M < 130M_\odot$ and a lower mass gap for $M < 5M_\odot$. The different scenarios considered in this paper are summarized in Table 1.

3. CONSTANT KERNEL EVOLUTION

First, we study the evolution of the BHMF assuming that the kernel $K(M, M') = K$ is a constant. This assumption is equivalent to the statement that the merger probability of two BHs is independent of their masses. In order to calibrate the constant K , we enforce the condition that the merger rate is equal to the LIGO merger rate per cluster, R_{LIGO} . This is done by noting that the total number of mergers per unit time is

$$\begin{aligned} R_{\text{LIGO}} &= \int_0^\infty \int_0^\infty K(x, y) n(x, t) n(y, t) dx dy \\ &= K \times N_{\text{BH}}^2, \end{aligned} \quad (2)$$

where N_{BH} is the number of BHs in the cluster. To estimate the LIGO rate per cluster, we adopt $\sim 10^{-2}$ per comoving Mpc^3 as the number density of Milky Way-like galaxies (Montero-Dorta & Prada 2009). Adopting $100 \text{ Gpc}^{-3} \text{ yr}^{-1}$ as a fiducial LIGO inferred merger rate gives the LIGO Galactic merger rate to be $N_{\text{MWEG}} \sim 10^{-5} R_{100}$ mergers per galaxy per year. For R_{tot} being the reported LIGO rate, the LIGO rate per cluster is therefore given by

$$\begin{aligned} R_{\text{LIGO}} &= \frac{R_{\text{tot}}}{N_C N_{\text{MWEG}}} \\ &= 10^{-5} \left[\frac{R_{\text{tot}}}{100 \text{ Gpc}^{-3} \text{ yr}^{-1}} \right] \left[\frac{1}{N_C} \right] \text{ yr}^{-1}, \end{aligned} \quad (3)$$

where N_C is the number of star clusters per galaxy.

3.1. No ejections

The simplest system we can study using this formalism is obtained by setting $S(M, t) = 0$ in Equation (1). This is equivalent to saying that the BHs exist in a closed system, and that no mergers are violent enough to eject

N_{BH}	R_{tot} [100 Gpc ⁻³ yr ⁻¹]	N_C	f_{ej}	Kernel	Figure Number
1000	100	100	0	Constant	Figure 1 (top)
1000	300	33	0	Constant	Figure 1 (bottom)
100	100	100	0	Constant	Figure 3
1000	300	33	0.5	Constant	Figure 4 (top)
1000	300	33	0.9	Constant	Figure 4 (middle)
1000	300	1	0.9	Constant	Figure 4 (bottom)
1000	100	100	0.9	Equation (7)	Figure 5
1000	10	100	0.5	Equation (8)	Figure 6

Table 1. List of parameters for the different scenarios under consideration in this paper. N_{BH} is the number of BHs per cluster, R_{tot} is the cosmological LIGO rate, N_C is the number of clusters per galaxy, f_{ej} is the ejection fraction, and Kernel denotes the coagulation kernel we used.

BHs out of the system. This situation is expected in cases where the star cluster is massive enough that the merger kick velocities are small compared to the escape velocity, e.g. for a star cluster at the core of a galaxy. Regardless of its limited usability, this simple case illustrates a lot of general features that are also present in more complicated cases.

3.1.1. Effects of the mass gaps on the BHMF

The lower mass gap (LG), and the upper mass gap (UG) (see Figure 1) affect the mass function evolution and produce features at various scales. First, the absence of BHs in the LG reduces the number of BHs of all scales. This is because no BH beyond the LG can merge with BHs in the LG to produce a more massive BH. The size of this reduction depends on the size of the LG, but is degenerate with the normalization of the IMF. As such, it is difficult to conclude anything about the LG, or even infer its existence, through this phenomenon.

Due to the self-similar nature of the constant coagulation kernel, one might expect that the resulting BHMF to also be self-similar. However, the gaps in the IMF spoils this self-similarity. The plots of Figure 1 display a break at $M \sim 10M_\odot$, which we call the lower break (LB). This break is caused because the BH formation channel where two BHs within the LG merge to form a BH beyond the LG is missing. Because the largest BH that could be formed by this channel is twice the largest BH in the LG, the LB is located at $M = 2M_{\max LG}$, where the largest BH in the LG, $M_{\max LG} = 5M_\odot$. Changing $M_{\max LG}$ results in pushing the LG to larger masses. If detected, the existence of the LB can be used to diagnose both the existence and size of the LG.

The interaction of the LG and the UG generates a break at $M \sim 60M_\odot$ in Figure 1. Because the most massive BHs in the IMF cannot merge with BHs in the LG, there is a dearth of BHs of mass $M_{\min UG} < M < (M_{\min UG} + M_{\max LG})$, where $M_{\min UG}$ is the most mas-

sive BHs in the IMF (the start of the UG). As the mass scale of the UB encodes the mass scale of the LG, an observation of the UB can be used to indirectly measure the size of LG.

The dearth of BHs that caused the LB and UB is also responsible to generating many more weaker breaks. Through a similar mechanism as was discussed in the previous paragraphs, anytime there is a dearth of BHs over a certain mass scale, there is a break due to there being fewer mergers than if the dearth is not present. However, these successive breaks are very weak, and are most probably not observable. Figure 2 depicts all of the missing channels discussed in this section.

3.1.2. Effects of varying the number of BHs per cluster

Because the merger rate is calibrated to the observed LIGO rate, clusters containing fewer BHs need to have more efficient mergers than clusters containing more BHs. This is manifested in Equation (2) as

$$K \propto \frac{1}{N_{BH}^2}. \quad (4)$$

Due to this increase in efficiency, for the same LIGO rate, clusters can develop a flat BHMF if they contain few BHs. Figure 3 shows the evolution of the BHMF over 10 Gyr with the same R_{LIGO} as the first plot of Figure 1 with $N_{BH} = 100$. If one assumes that the BHMF is a power law, then situations as shown in Figure 3 have to be excluded. Assuming a R_{LIGO} of 10^{-5} yr⁻¹ and $N_C = 10$ requires each cluster to contain at minimum ~ 1000 BHs.

3.2. Evolution with ejections

In the process of assembling a dynamical binary, or due to the merger kicks experienced by a merged BH, a star cluster is continuously losing BHs. We model the ejection of BHs from the system by introducing a source function, $S(M, t)$, that reduces the number of BHs of

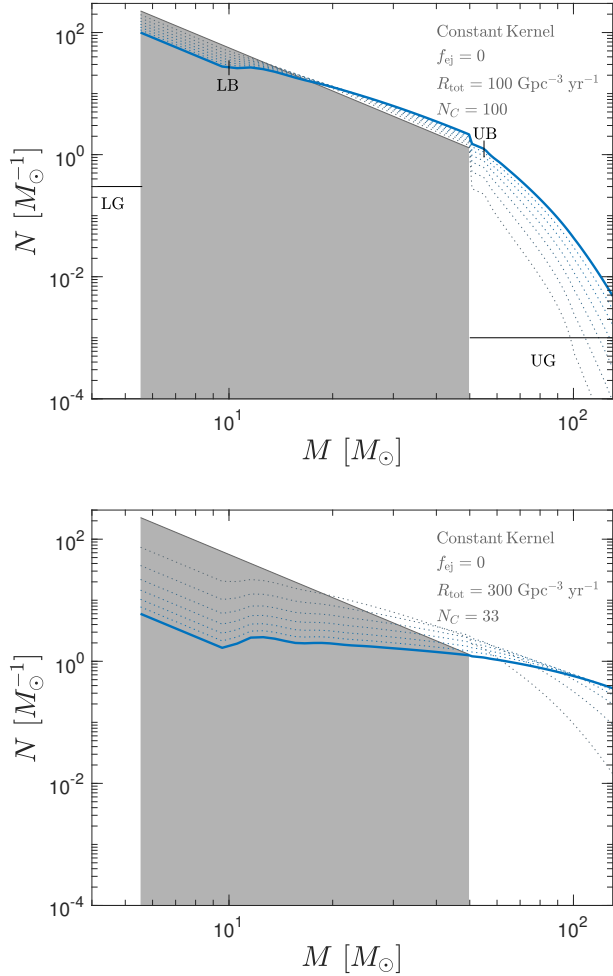


Figure 1. The evolution of the BHMF starting from the IMF (black) to 10 Gigayears (solid blue) for a cluster with 1000 BHs. Dotted blue lines represent the BHMF at intervening times. The top figure shows evolution of the mass function with a LIGO rate of $100 \text{ Gpc}^{-3} \text{ yr}^{-1}$ and the number of clusters per MWEG to be $N_C = 100$, while the lower figure shows evolution of the mass function with a LIGO rate of $300 \text{ Gpc}^{-3} \text{ yr}^{-1}$ and $N_C = 33$, i.e. a LIGO rate *per cluster* that is ~ 10 times higher. Varying N_C is equivalent to changing the LIGO rate by the reciprocal factor.

mass M by a number that is proportional to the amount of mergers that produce BHs of mass M ,

$$S(M, t) = -\frac{f_{\text{ej}}}{2} \int_0^M K(M - M', M') N(M - M', t) N(M', t) dM', \quad (5)$$

where f_{ej} is the ejected fraction. In effect, this source function parameterizes the phenomenon that for every merger, a fraction f_{ej} of the BHs are ejected. While we kept the parameter f_{ej} as a single number, in reality the

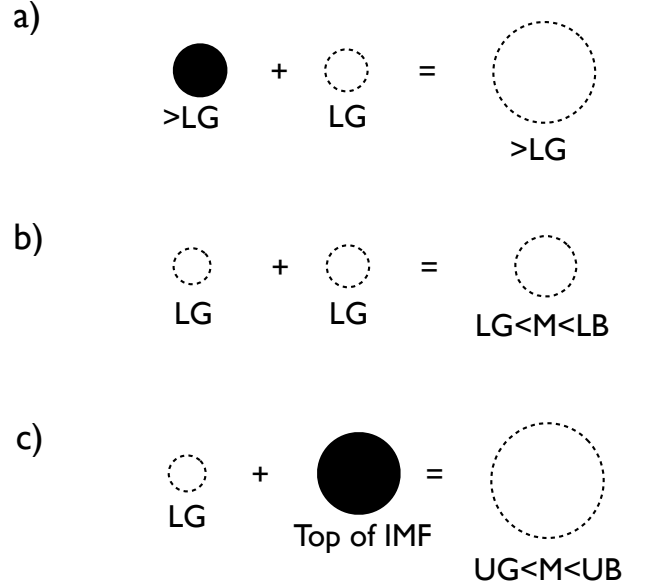


Figure 2. Missing BH formation channels due to the existence of the lower mass gap (LG) and the upper mass gap (UG). Case (a) shows that the number of BHs at all scales are lowered because no BH can merge with BHs in the LG to form a larger BH. Case (b) depicts the missing channel responsible for the break at $M = 10 M_\odot$ in Figure 1, which we call the lower break (LB). Because BHs generated by the mergers of two BHs within the LG is missing, there is a dearth of BH of mass $5 M_\odot < M < 10 M_\odot$. Case (c) shows the missing channel that results from the interaction of LG and UG. Because BHs from the top of the IMF cannot merge with BHs within LG, there is a dearth of BHs with mass $50 M_\odot < M < 60 M_\odot$, causing the break at $M = 60 M_\odot$ in Figure 1.

recoil kicks of binary BHs depend on the spins of the individual BHs. For simplicity, we will neglect the spin dependence of f_{ej} .

Note that this parameterization is agnostic towards the actual ejection mechanism. For a given merger, the two BHs that participate in the merger event can be kicked out during their assembly process, or the two BHs can merge, producing a gravitational wave recoil that ejects the merged BH from the cluster. Figure 4 shows the evolution of the BHMF for a cluster with an ejection fraction of $f_{\text{ej}} = 0.5$ and $f_{\text{ej}} = 0.9$.

There are a few main differences between a cluster without ejections and a cluster with efficient ejections. First, ejections lower the normalization of the BHMF, as there are less BHs at all scales. Next, ejections prevent the BHMF from being flattened. Indeed, as shown in the bottom plot of Figure 4, even a scenario with a merger rate at the top of the LIGO range ($R_{\text{tot}} = 300 \text{ Gpc}^{-3} \text{ yr}^{-1}$) fails to flatten the BHMF if f_{ej} is allowed to be

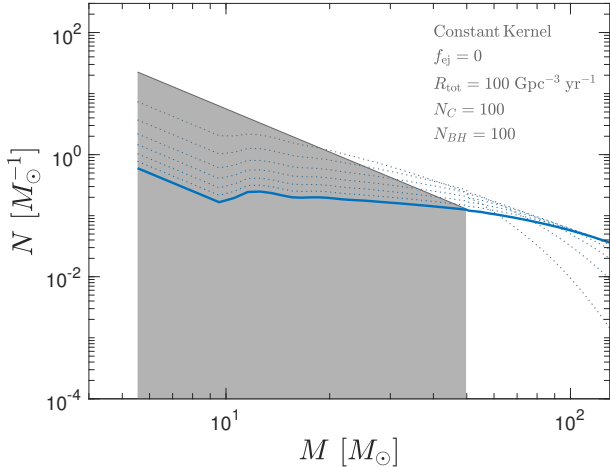


Figure 3. The evolution of the BHMF starting from the IMF (black) to 10 Gigayears (solid blue) for a cluster with 100 BHs. Dotted blue lines represent the BHMF at intervening times. The LIGO rate is taken to be $100 \text{ Gpc}^{-3} \text{ yr}^{-1}$, and the number of clusters per MWEG is taken to be $N_C = 100$. Lowering the number of BHs per cluster flattens the BHMF in a similar way as increasing the LIGO rate.

very high. This allows clusters with low number of BHs ($N_{\text{BH}} < 100$), or scenarios with very high merger rate per cluster to be consistent with the cutoff at $\sim 40M_\odot$.

In addition to the global properties described in the previous paragraph, efficient ejections also change the properties of the BHMF at certain scales. The LB turns into a step function when ejections are efficient, which might make its detection in the BHMF difficult. As seen in Figure 4, for the first few Gigayears, there is now a discontinuity at the end of the UB. Because channel (c) in Figure 2 is missing, BHs with masses $50M_\odot < M < 60M_\odot$ (those between the start of the UG and the UB) are generally formed by fewer mergers than BHs generated beyond the UB. As for every merger there is a chance to be ejected out of the systems, BHs beyond the UB suffer more ejections than those below the UB. This discontinuity is a signature that the system is efficiently ejecting their BHs, and the drop is larger for higher f_{ej} . However, the evolution of the coagulation equation tends to smooth out discontinuities, and the magnitude of the drop is heavily suppressed after 10 Gyrs.

4. EVOLUTION WITH TOP-HEAVY KERNELS

Many phenomena responsible for dynamical mergers, such as gravitational capture, mass segregation, and 3-body relaxation are mass dependent. Therefore, we would expect that the coagulation kernel in equation (1) is in reality a function of mass, $K = K(M, M')$. While the actual form of the coagulation kernel depends on the

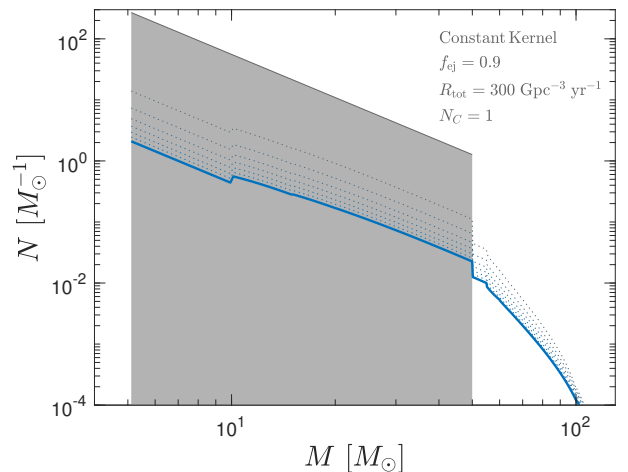
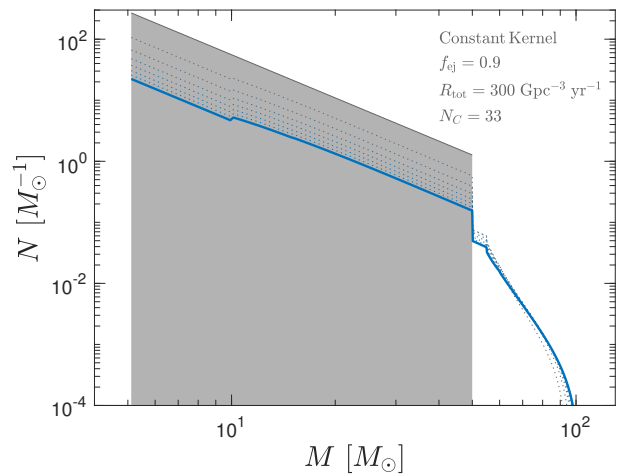
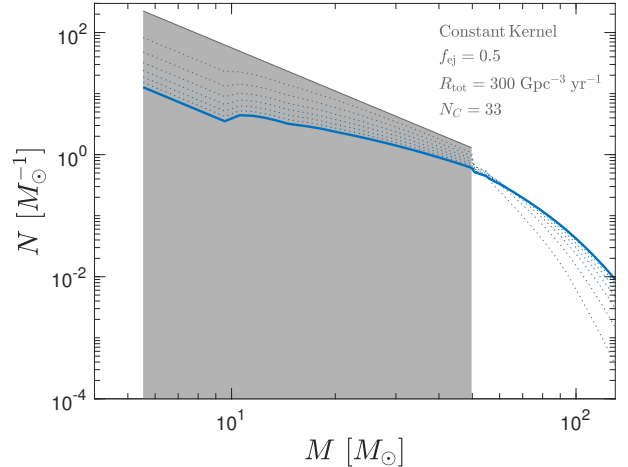


Figure 4. The evolution of the BHMF starting from the IMF (black) to 10 Gigayears (solid blue) for a cluster with 1000 BHs. Dotted blue lines represent the BHMF at intervening times. The LIGO rate is taken to be $300 \text{ Gpc}^{-3} \text{ yr}^{-1}$, and the number of clusters per MWEG is taken to be $N_C = 33$ (top, middle) and $N_C = 1$ (bottom). The ejection fraction is taken to be $f_{\text{ej}} = 0.9$. Even for a LIGO rate per cluster of $300 \text{ Gpc}^{-3} \text{ yr}^{-1}$, the BHMF fails to flatten in 10 Gigayears.

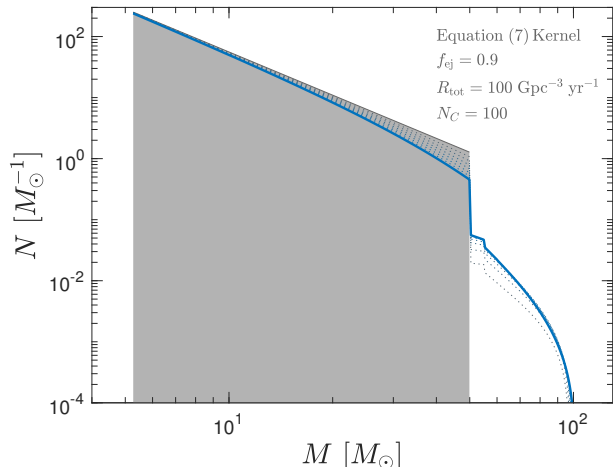


Figure 5. The evolution of the BHMF starting from the IMF (black) to 10 Gigayears (solid blue) for a cluster with 1000 BHs for the top-heavy coagulation kernel given by equation (7). Dotted blue lines represent the BHMF at intervening times.. The LIGO rate is taken to be $100 \text{ Gpc}^{-3} \text{ yr}^{-1}$, and the number of clusters per MWEG is taken to be $N_C \sim 100$. The ejection fraction is taken to be $f_{ej} = 0.9$.

dominant merging mechanism, it has to be symmetrical with respect to M and M' . In general, this symmetry along with physical considerations forces the functional form of the coagulation kernel to be

$$K \propto (MM')^\alpha (M + M')^\beta, \quad (6)$$

with power-law indices α and β . The effectiveness of gravitational processes increases with increasing mass. Gravitational capture, for example, is more efficient for larger M and M' . This implies that heavier BHs merge preferentially, and that K is top-heavy. For example, the coagulation kernel due to gravitational radiation capture scales as (Mouri & Taniguchi 2002)

$$K_{\text{cap}} \propto (MM')^{15/14} (M + M')^{9/14}. \quad (7)$$

Figure 5 shows the evolution of the BHMF with the coagulation kernel given by equation (7). While the specific values of α and β would matter for the numerical values of f , the salient features of the calculation is valid for general top-heavy kernels. The most important change introduced by the top-heavy kernel is the lost of the power-law behavior in the mass range $5M_\odot < M < 50M_\odot$.

Another example is the coagulation kernel from 3-body relaxation, which is computed through numerical simulations to scale as (O’Leary et al. 2016)

$$K_{3\text{-body}} \propto (M + M')^4. \quad (8)$$

However, Ref. O’Leary et al. (2016) did not fit for the $(MM')^\alpha$ component. In the coagulation equation, the $(MM')^\alpha$ term acts as a regularizer, and its absence generates a runaway growth of BHs that concentrates most of the cluster’s mass in a single BH of extremely large mass $M \gtrsim 1000M_\odot$. Observationally, we do not see such runaway growth. Thus, in order for this kernel to be consistent with observational bounds in the absence of the $(MM')^\alpha$ term, there must be some maximum M_{max} above which this kernel is suppressed. We impose this regularization by setting the kernel to be $(M_{\text{max}} + M')^4$ for $M > M_{\text{max}}$. While this introduces a new parameter to the problem, Figure 6 shows that even a very conservative choice of $M_{\text{max}} = 100M_\odot$, a significant population of BHs can be formed within the UG. Indeed, the use of this kernel does not change the main qualitative features of the other kernels, which is the possibility of intermediate mass BH seed formation in dynamical clusters. This echoes a previous result showing that in nuclear star clusters it is possible to obtain BHs in the intermediate mass ranges through multiple mergers (Antonini & Rasio 2016). Our calculations extend this conclusion to the statement that globular clusters are also capable of producing intermediate mass BHs.

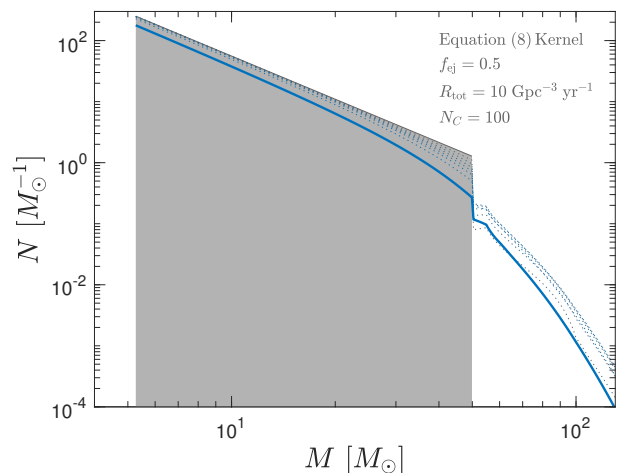


Figure 6. The evolution of the BHMF starting from the IMF (black) to 10 Gigayears (solid blue) for a cluster with 1000 BHs for the 3-body coagulation kernel given by equation (8). Dotted blue lines represent the BHMF at intervening times.. The LIGO rate is taken to be $10 \text{ Gpc}^{-3} \text{ yr}^{-1}$, and the number of clusters per MWEG is taken to be $N_C \sim 100$. The ejection fraction is taken to be $f_{ej} = 0.5$ and $M_{\text{max}} = 100M_\odot$.

5. CONCLUSION

Through evolving a coagulation equation, we have shown that the BHMF in clusters could evolve to fill the

gap in the IMF of BHs at $50M_{\odot} < M < 130M_{\odot}$. Further, we have found that the upper range of the LIGO rate is not consistent with the dearth of BHs with masses $M > 40M_{\odot}$ reported by Fishbach & Holz (2017) unless ejection is efficient. The coagulation equation also implies that the mass gap between the most massive neutron stars and the least massive BHs produces potentially observable features at larger scales. In addition, we show that that for top-heavy kernels, the mass function between $5M_{\odot} < M < 50M_{\odot}$ is driven away from self-similarity, and that a power-law will not be sufficient to fit the BHMF in this regime. With parameters consistent with realistic globular clusters, we showed that it is

possible to form intermediate BH seeds through mergers of smaller BHs.

ACKNOWLEDGEMENTS

The authors would like to thank the anonymous referee, Chris Belczynski, and Tuguldur Sukhbold for comments on the manuscript. Support (PM) for this work was provided by NASA through Einstein Postdoctoral Fellowship grant number PF7-180164 awarded by the *Chandra* X-ray Center, which is operated by the Smithsonian Astrophysical Observatory for NASA under contract NAS8-03060. This work was supported in part by Harvard’s Black Hole Initiative, which is funded by a grant from the John Templeton Foundation.

REFERENCES

- Abbott, B. P., Abbott, R., Abbott, T. D., et al. 2016a, *Physical Review Letters*, 116, 241103
- . 2016b, *Physical Review Letters*, 116, 061102
- . 2017a, *Physical Review Letters*, 118, 221101
- . 2017b, *ApJL*, 851, L35
- . 2017c, *Physical Review Letters*, 119, 141101
- Antonini, F., & Rasio, F. A. 2016, *ApJ*, 831, 187
- Bai, Y., Barger, V., & Lu, S. 2018, ArXiv e-prints, arXiv:1802.04909
- Belczynski, K., Bulik, T., Fryer, C. L., et al. 2010a, *ApJ*, 714, 1217
- Belczynski, K., Dominik, M., Bulik, T., et al. 2010b, *ApJL*, 715, L138
- Belczynski, K., Wiktorowicz, G., Fryer, C. L., Holz, D. E., & Kalogera, V. 2012, *ApJ*, 757, 91
- Belczynski, K., Heger, A., Gladysz, W., et al. 2016, *A&A*, 594, A97
- Dominik, M., Berti, E., O’Shaughnessy, R., et al. 2015, *ApJ*, 806, 263
- Farr, W. M., Sravan, N., Cantrell, A., et al. 2011, *ApJ*, 741, 103
- Fishbach, M., & Holz, D. E. 2017, *ApJL*, 851, L25
- Fishbach, M., Holz, D. E., & Farr, B. 2017, *ApJL*, 840, L24
- Gerosa, D., & Berti, E. 2017, *PhRvD*, 95, 124046
- Keck, D. D., & Bortz, D. M. 2013, ArXiv e-prints, arXiv:1312.7240
- Kreidberg, L., Bailyn, C. D., Farr, W. M., & Kalogera, V. 2012, *ApJ*, 757, 36
- Montero-Dorta, A. D., & Prada, F. 2009, *MNRAS*, 399, 1106
- Mouri, H., & Taniguchi, Y. 2002, *ApJL*, 566, L17
- O’Leary, R. M., Meiron, Y., & Kocsis, B. 2016, *ApJL*, 824, L12
- O’Leary, R. M., Rasio, F. A., Fregeau, J. M., Ivanova, N., & O’Shaughnessy, R. 2006, *ApJ*, 637, 937
- Özel, F., Psaltis, D., Narayan, R., & McClintock, J. E. 2010, *ApJ*, 725, 1918
- Raithel, C. A., Sukhbold, T., & Özel, F. 2017, ArXiv e-prints, arXiv:1712.00021
- Rodriguez, C. L., Amaro-Seoane, P., Chatterjee, S., & Rasio, F. A. 2017, ArXiv e-prints, arXiv:1712.04937
- Rodriguez, C. L., Chatterjee, S., & Rasio, F. A. 2016a, *PhRvD*, 93, 084029
- Rodriguez, C. L., Haster, C.-J., Chatterjee, S., Kalogera, V., & Rasio, F. A. 2016b, *ApJL*, 824, L8
- Rodriguez, C. L., Morscher, M., Pattabiraman, B., et al. 2015, *Physical Review Letters*, 115, 051101
- Salpeter, E. E. 1955, *ApJ*, 121, 161
- Samsing, J., D’Orazio, D. J., Askar, A., & Giersz, M. 2018, ArXiv e-prints, arXiv:1802.08654
- Smoluchowsky, M. 1916, *Physik. Z.*, 17, 557
- Sukhbold, T., Ertl, T., Woosley, S. E., Brown, J. M., & Janka, H.-T. 2016, *ApJ*, 821, 38
- Woosley, S. E. 2017, *ApJ*, 836, 244

APPENDIX

A. COAGULATION EQUATION NUMERICAL SOLVER

The coagulation equation is solved using a finite volume method based on [Keck & Bortz \(2013\)](#). The coagulation equation can be written in conservative form as a function of $G(M, t) \equiv M \times N(M, t)$:

$$\partial_t G + \partial_M J(G) = MS \quad (\text{A1})$$

where

$$J(G) = \int_0^M \int_{M-u}^{M_{\max}} \frac{K(u, v)}{v} G(t, u) G(t, v) dv du \quad (\text{A2})$$

is the mass flux across mass bins. G is a conserved quantity in the absence of source terms and conserved by our numerical finite-volume method.

The solution is discretized into mass bins and in time as $G_i^N(t_k)$ which represents the mean value of $G(t_k, M)$ in the mass bin $[M_i, M_{i+1})$ at time t_k . The mass bin has center $M_{\text{mid}(i)}$. The left boundary flux is zero: $J_1^N(t_k) = 0$. In general, the flux $J_r^N(t_k)$ across each discrete boundary x_r can be computed as follows, by considering the aggregation of $M_{\text{mid}(i)}$ and $M_{\text{mid}(j)}$. For each fixed r , and a fixed i such that $M_{\text{mid}(i)} < M_r$, then each j such that $M_{\text{mid}(j)} \geq M_r - M_{\text{mid}(i)}$ gives a contribution to the flux of:

$$\Delta x G_i^N(t_k) \int_{M_j}^{M_{j+1}} \frac{K(M_{\text{mid}(i)}, y)}{y} G_j^N(t_k) dy \quad (\text{A3})$$

A small exception occurs for the lowest j , where the lower limit of integration is $M_{\text{mid}(j)}$ instead of M_j . The integral is evaluated for an arbitrary kernel numerically using a quadrature rule.

The equations are explicitly evolved from time step t_k to t_{k+1} as:

$$G_i^{N'} = G_i^N(t_k) + (\Delta t/2) \times M_i S_i(t_k, G_i^N(t_k)) \quad (\text{A4})$$

$$G_i^{N''} = G_i^{N'} + \Delta t \frac{J_{i+1}^N - J_i^N(t_k)}{\Delta x} \quad (\text{A5})$$

$$G_i^N(t_{k+1}) = G_i^{N''} + (\Delta t/2) \times M_i S_i(t_k, G_i^{N''}) \quad (\text{A6})$$

that is, adding the source term in two half-steps which sandwich the flux term to result in a second-order method.